*Semiconductor Physics, Quantum Electronics & Optoelectronics, 2024. V. 27, No 4. P. 457-465.*

*Optoelectronics and optoelectronic devices*

# Si-based $n^{++}$-$p^{-}$-$p^{+}$-$p^{-}$-$p^{++}$ avalanche diode: Self-consistent modeling for infrared optoelectronic applications

**S.V. Sapon[1], B.M. Romaniuk[1], V.P. Melnik[1], O.V. Dubikovskyi[1], O.A. Kulbachynskyi[1], O.S. Oberemok[1], Z.V. Maksimenko[1], O.V. Kosulya[1], V.V. Korotyeyev[1], V.N. Sokolov[1], A.V. Bychok[2]**

[1]*V. Lashkaryov Institute of Semiconductor Physics, 41 Nauky Avenue, 03028 Kyiv, Ukraine*
[2]*State enterprise "State research institute "Orion", 03057 Kyiv, Ukraine*
*Corresponding author e-mail: koroteev@ukr.net*

**Abstract.** A theoretical approach for modeling electric and photoelectric characteristics of specifically designed Si-based $n^{++}$-$p^{-}$-$p^{+}$-$p^{-}$-$p^{++}$ avalanche photodiodes has been developed. The electrostatic characteristics (band bending, built-in electrostatic fields and carrier distributions) and current-voltage characteristics including photocurrent and diode sensitivity to electromagnetic radiation of the near-infrared spectral range have been calculated and analyzed for the room operation temperature. The measured doping profiles in the fabricated prototype of the avalanche Si-based photodiode have been used in the calculations. For a particular set of the photodiode parameters, we have found that the avalanche transport regime occurs at the applied reverse voltage of ~ –47 V across the diode length of 380 μm We have established that the rapid exponential growth of the current densities from 0.01 to 100 μA/cm$^2$ in the range of the applied voltages of –40 to –47 V is inherent for formation of the avalanche-type transport regime. At this, considerable photoresponsibility values of 100 to 30 A/W are predicted for electromagnetic radiation wavelengths of 0.8 to 1 μA. All the results have been obtained using literature data on field dependences of the impact ionization coefficients, spectral dependences of the optical permittivity (refractive index and extinction coefficient), *etc*.

**Keywords:** Si-based photodiode, current-voltage characteristics, photoresponse, implantation.

https://doi.org/10.15407/spqeo27.04.457
PACS 61.72.uj, 85.30.Kk, 85.60.Dw

Manuscript received 02.10.24; revised version received 26.10.24; accepted for publication 13.11.24; published online 06.12.24.

## 1. Introduction

Avalanche *p-n* diodes designed for optoelectronic applications, such as detectors of electromagnetic radiation, are characterized by existence of a carrier-multiplication (avalanche) region formed due to impact ionization of crystal atoms by the drifting carriers. This essentially distinguishes the operation of such diodes from that of ordinary photodiodes [1, 2]. The properties and output characteristics of avalanche photodiodes (APDs) are defined by the sum of two contributions originating from the carrier-multiplication avalanche process and the process typical for ordinary photodiodes. Since the carrier avalanche is initiated at very high electric fields, at which electron-hole multiplication takes place, the interband Ziner tunneling may be a concurrent process. However, it has been well recognized that silicon and germanium are preferable materials for APDs because the tunneling current in such indirect bandgap semiconductors is much lower than that for the direct bandgap case and, hence, the avalanche process dominates over the tunneling at high electric fields up to the field strength of $10^6$ V/cm [3]. In particular, this leads to silicon APDs with a low dark current.

The principle of operation of APDs is based on two physical phenomena: (i) the internal photoelectric effect, and (ii) avalanche multiplication of charge carriers, namely electrons and holes, initiated by impact ionization in a reverse-biased *p-n* junction created in the APD. Since these both electronic phenomena are very fast and, in addition, the RC-factor of an electric circuit may be rather low, the APDs are used as very sensitive and fast photodetectors [1, 2]. As the energy gap, $\varepsilon_g$, between the conduction and the valence band in silicon is about 1 eV ($\varepsilon_g$ = 1.15 eV at 300 K), the APDs are developed and optimized for detecting visible and near infrared (IR) radiation with the wavelengths in the range from 400 nm to 1100 nm.

An incident photon flux $Q$ decays with increasing the distance $x$ from the diode photosensitive area into the

semiconductor bulk, $Q(x)=Q_0\exp(-\alpha x)$, where α is the absorption coefficient at a given wavelength. The absorbed photon flux causes generation of electron-hole pairs, which are separated in a reverse-biased junction of the photodetector structure thereby providing the corresponding electric photoresponse in the external electric circuit. Hence, in order to achieve the highest photodiode sensitivity, the absorption region should be sufficiently thick – most often it is considered to exceed 2/α. At the same time, the reflection index of the surface receiving an incident flux should be as low as possible, which may be achieved by coating with an effective antireflection film.

In a theoretical description of an avalanche *p-n* diode, the effect of carrier multiplication due to impact ionization is taken into account by introducing in the continuity equations for the electron and hole current densities $j_n$ and $j_p$:

$$\frac{dj_n}{dx}=-\frac{dj_p}{dx}=\ldots-g(E), \tag{1}$$

the respective generation term

$$g(E)=\alpha_n(E)|j_n|+\alpha_p(E)|j_p|. \tag{2}$$

Here, $\alpha_n(E)$ and $\alpha_p(E)$ are the impact ionization coefficients (or ionization rates) for electrons (*n*) and holes (*p*), both of them being dependent on the electric field *E*. The generation term is also proportional to the electron and hole current densities, $j_n=env_n$ and $j_p=env_p$ [4], where *n*, *p*, $v_n$, and $v_p$ are the electron and hole concentrations and velocities, respectively, and *e* is the elementary charge. The minus sign in Eq. (1) takes into account that electrons and holes move in opposite directions (we accept that the holes move in the positive direction of the *x*-axis). The function *g*(*E*) defines the number of electron-hole pairs created by impact ionization. The ionization rate of carriers with the velocity *v* may be written in a general form as follows [5]:

$$\alpha(E)=\frac{1}{v(E)}\int_0^\infty v_i(\epsilon)f(\epsilon,E)d\epsilon\approx\alpha_0(\epsilon_i,E)\int_{\epsilon_i}^\infty f(\epsilon,E)d\epsilon, \tag{3}$$

where $v_i(\epsilon)$ is the ionization probability for a carrier with the energy $\epsilon$, $\epsilon_i$ is the ionization energy, and $f(\epsilon,E)$ is the distribution function, respectively. The prefactor $\alpha_0(\epsilon_i,E)=v_i(\epsilon_i)/v(E)$ has the dimensionality [cm$^{-1}$], so that $1/\alpha_0(\epsilon_i,E)=L_i(\epsilon_i,E)$ is the characteristic ionization length, *i.e.* the mean-free path relative to ionization of a carrier with an energy greater than $\epsilon_i$. The explicit expression for $\alpha_0(\epsilon_i,E)$ is given by [5]

$$\alpha_0(\epsilon_i,E)=\frac{eE}{r_i\times\eta\omega_{op}+\epsilon_i}\ . \tag{4}$$

Here, $\hbar\omega_{op}$ is the optical phonon energy, $r_i=L_i/L$, $L$ is the carrier mean-free path relative to scattering by optical phonons, which is assumed to be the dominant scattering mechanism for carriers with energies greater than $\hbar\omega_{op}$. These three quantities $r_i$, $\epsilon_i$, and $\hbar\omega_{op}$ are considered to be the model adjustable parameters, which should be found by comparing the calculation results with appropriate experimental data. These quantities differ for different semiconductor materials.

It should be noted that knowledge of the field dependence of the ionization rates of mobile charge carriers in semiconductors used for development of avalanche *p-n* diodes is of primary importance for prediction and adequate theoretical description of the carrier transport as well as the device output performance. Eqs. (3) and (4) provide an approximate field dependence of the ionization rates and their relation to the characteristic semiconductor parameters: the optical phonon energy, the ionization energy of intrinsic lattice, and the carrier mean-free path and the ionization length (or their ratio). In addition to the mentioned adjustable parameters, asymptotic dependence of the distribution function on the electric field in Eq. (3) should be calculated. The required parameters are determined by comparing the calculated dependences with available experimental data. In this paper, we have used the results for the field dependences of the ionization rates provided in [2, 4], which have been obtained by the best fit for silicon *p-n* avalanche diodes. It is worth noting that development of a theory of impact ionization, which would allow calculation of the ionization rates in specific semiconductors, is a difficult problem. Therefore, such theories still contain simplifying assumptions, *e.g.* they neglect the multivalley anisotropic band structure. In silicon, the electron multivalley band structure is characterized by the existence of six anisotropic valleys in the conduction band with essentially different effective masses along and perpendicular to the long valley axis. This important feature can entirely determine the asymptotic shape of the distribution function in strong electric fields [6, 7]. In the framework of the theoretical approach, the effective field acting on electrons in different valleys of Si is equivalent for the electric field direction along (111) crystallographic axis. Therefore, no angular dependence of the electron ionization rate with regard to rotation around the (111) axis is expected. In this case all the valleys are oriented symmetrically relative to the electric field direction.

The paper is organized as follows. The transport model and basic equations are presented in Section 2. The results of the calculations of steady-state characteristics are discussed in Section 3. The photoelectric characteristics, including the analysis of the avalanche diode responsivity, are provided in Section 4. Section 5 summarizes the basic results of the paper.

## 2. Modeling the Si-based $n^{++}$-$p^{-}$-$p^{+}$-$p^{-}$-$p^{++}$ avalanche diode

To analyze the basic electric characteristics of the avalanche diode, we used a simplified approach, considering a spatially inhomogeneous one-dimensional problem. The proposed theoretical model [8] is based on solving together the Poisson equation (Eq. (5a)), which includes the relationship between the electrostatic potential ϕ(*x*) and the electric field *E*(*x*) (Eq. (5b)), the transport equations for the electron, $j_n$, and hole, $j_p$,

current densities (Eqs. (5c) and (5d), respectively) written in the framework of the drift-diffusion model, and the continuity equations (Eqs. (5e) and (5f)):

$$\frac{d^2\phi(x)}{d^2x} = \frac{4\pi e}{\kappa_0}\left[n(x) - p(x) - N_d(x) + N_a(x) + p^-\right], \quad (5a)$$

$$E(x) = -\frac{d\phi(x)}{dx}, \quad (5b)$$

$$j_n(x) = \mu_n n(x)\frac{d\varepsilon_{\mathrm{F},n}(x)}{dx}, \quad (5c)$$

$$j_p(x) = \mu_p p(x)\frac{d\varepsilon_{\mathrm{F},p}(x)}{dx}, \quad (5d)$$

$$\frac{1}{e}\frac{dj_n(x)}{dx} = \Gamma\left[n(x)p(x) - n_0 p_0 N_d(x)\right] - \left[\alpha_n(E(x))\left|j_n(x)\right| + \alpha_p(E(x))\left|j_p(x)\right|\right], \quad (5e)$$

$$\frac{dj_n(x)}{dx} = -\frac{dj_p(x)}{dx}. \quad (5f)$$

In Eq. (5a), $n(x)$ and $p(x)$ are the electron and hole concentrations, $N_d(x)$ and $N_a(x)$ are the spatial profiles of the donor and acceptor doping, respectively, $p^-$ is the background hole concentration in the weakly $p$-doped unprocessed silicon wafer, and $\kappa_0$ is the static dielectric permittivity, respectively. The current densities in the transport equations (5c) and (5d) are expressed through the spatial derivatives of the quasi-Fermi levels, $\varepsilon_{\mathrm{F},n}(x)$ for electrons and $\varepsilon_{\mathrm{F},p}(x)$ for holes. $\mu_{n,p}$ are the electron and hole mobilities, respectively. On the right-hand side of the continuity equation (5e), the first term describes the band-to-band generation-recombination processes of electron-hole pairs. Here, $n_0$ and $p_0$ are the equilibrium electron and hole concentrations, and $\Gamma$ is the bulk recombination coefficient, respectively. The second term describes the effect of carrier generation due to the impact ionization. Here, $\alpha_n$ and $\alpha_p$ are the corresponding impact ionization coefficients discussed in Section 1.

The concentrations $n(x)$ and $p(x)$ are related to the potential $\phi(x)$ and the corresponding quasi-Fermi levels $\varepsilon_{\mathrm{F},n}$ and $\varepsilon_{\mathrm{F},p}$ as follows:

$$n(x) = N_c F_{1/2}\left(\left[\varepsilon_{\mathrm{F},n}(x) + e\phi(x)\right]/k_{\mathrm{B}}T\right) \quad (6a)$$

$$p(x) = N_v F_{1/2}\left(\left[-\varepsilon_{\mathrm{F},p}(x) - e\phi(x) - \varepsilon_g\right]/k_{\mathrm{B}}T\right). \quad (6b)$$

Here, $T$ is the ambient temperature, $k_{\mathrm{B}}$ is the Boltzmann constant, the function $F_{1/2}(x)$ is the Fermi–Dirac integral of half-integer order, $N_{c,v} = 2^{1/2} m_{c,v}^{3/2} (k_{\mathrm{B}}T)^{3/2}/\pi^2\eta^3$ are the effective densities of states in the conduction ($c$) and valence ($v$) band, respectively, and $m_{c,v}$ are the electron and the hole effective masses for the density of states. Eq. (5f) implies that the total current density is constant across the whole diode, *i.e.*

$$j = j_n(x) + j_p(x) = \text{const}. \quad (7)$$

The system (5a)–(5f) is convenient to rewrite in the dimensionless form:

$$\begin{aligned}
&\frac{d\Phi}{dX} = E'(X),\\
&\frac{dE'(X)}{dX} = N'_c F_{1/2}\left(\xi_n(X) - \Phi(X)\right) + \\
&+ N'_v F_{1/2}\left(\Phi(X) - \xi_p(X) - \xi_g\right) + \\
&+ N'_d(x) - N'_a(x) - 1 \equiv \rho'(X)\\
&\frac{d\xi_n}{dX} = \frac{j'_n(X)}{N'_c F_{1/2}\left(\xi_n(X) - \Phi(X)\right)},\\
&\frac{d\xi_p}{dX} = \frac{\mu_n}{\mu_p}\frac{j'_p(X)}{N'_v F_{1/2}\left(\Phi(X) - \xi_p(X) - \xi_g\right)},\\
&\frac{j'_n(X)}{dX} = \Gamma'\left[\begin{array}{l} N'_c N'_v F_{1/2}\left(\xi_n(X) - \Phi(X)\right)\times \\ \times F_{1/2}\left(\Phi(X) - \xi_p(X) - \xi_g\right) - N'_0 P'_0 \end{array}\right] - \\
&- \left[\alpha'_n(E'(X))\left|j'_n(X)\right| + \alpha'_p(E'(X))\left|j'_p(X)\right|\right],\\
&\frac{dj'_n(X)}{dX} = -\frac{dj'_p(X)}{dX}.
\end{aligned} \quad (8)$$

We have also introduced the following dimensionless variables:

$$X = \frac{x}{L_{\mathrm{D}}},\ \Phi = -\frac{e\phi}{k_{\mathrm{B}}T},\ \xi_{\{n,p\}} = \frac{\varepsilon_{\mathrm{F},\{n,p\}}}{k_{\mathrm{B}}T},\ \xi_g = \frac{\varepsilon_g}{k_{\mathrm{B}}T},$$

$$E' = \frac{E}{E_{\mathrm{D}}},\ N'_{c,v} = \frac{N_{c,v}}{p^-},\ j'_{\{n,p\}} = \frac{j_{\{n,p\}}}{j_{\mathrm{D}}},$$

$$N'_0, P'_0 = \frac{n_0, p_0}{p^-},\ \alpha'_{\{n,p\}} = \alpha_{\{n,p\}} L_{\mathrm{D}},\ \Gamma' = \Gamma \times \frac{ep^- L_{\mathrm{D}}^2}{\mu_n k_{\mathrm{B}}T},$$

where $L_{\mathrm{D}} = \sqrt{\kappa_0 k_{\mathrm{B}}T/4\pi e^2 p^-}$ is the Debye screening length with respect to the background concentration $p^-$, $E_{\mathrm{D}} = k_{\mathrm{B}}T/eL_{\mathrm{D}}$, and $j_{\mathrm{D}} = ep^-\mu_n E_{\mathrm{D}}$.

The system (8) is a nonlinear system of six differential equations of first order, which should be supplemented by six boundary conditions at the diode edges:

$$\Phi(L'_b) = 0, \quad (9a)$$

$$\Phi(0) = \Phi_b + U'_b, \quad (9b)$$

$$\xi_n(L'_b) = \xi_p(L'_b) = \xi_{\mathrm{F}}, \quad (9c, 9d)$$

$$\xi_n(0) = \xi_p(0) = \xi_{\mathrm{F}} + U'_b. \quad (9e, 9f)$$

In Eqs. (9c)–(9f), $L'_b = L_b/L_{\mathrm{D}}$ and $U'_b = eU_b/k_{\mathrm{B}}T$ are the dimensionless diode length and external applied voltage in the units of $k_{\mathrm{B}}T/e$. The conditions expressed by Eqs. (9a)–(9f) assume that at the edges ($x = 0$, $x = L_b$) of the diode, electric charge neutrality and charge carriers equilibrium are supported by the contacts. These two unknown parameters, namely $\Phi_b$ – the built-in electrostatic potential and $\xi_{\mathrm{F}}$ – the Fermi level under equilibrium

($U'_b = 0$), should be found from the electrical neutrality conditions at the diode edges:

$$\rho'(0) = 0, \quad \rho'(L'_b) = 0. \qquad (10)$$

Thus, the system (8) and the boundary conditions (9a)–(9f) together with the neutrality conditions (10) finalize the mathematical approach for analyzing the electric characteristics of the considered *p-n* diode. The boundary value problem for the nonlinear system of equations (8) was numerically solved by the finite-difference method, which reduced Eqs. (8) to a system of nonlinear algebraic equations. The latter was solved using the Newton method with precise step control. This briefly described numerical procedure was implemented as a working subroutine in Fortran-source libraries.

### 3. Steady-state electric characteristics

The developed theoretical model was applied for determining the basic parameters and particular doping profiles of the fabricated Si-based avalanche diode.

The following parameters of the silicon diode were used in the calculations: $p^- = 2\times10^{12}$ cm$^{-3}$, $L_b = 380$ μm, $m_c = 6 \times 0.36m_e$ (here, $m_e$ is the free electron mass, the factor 6 takes into account the number of valleys), $m_v = 0.81m_e$, $\varepsilon_g = 1.1$ eV, $\kappa_0 = 11.7$, and $\mu_{n(p)} =$ = 1000 (500) cm$^2$/V·s (see Ref. [9]). All the calculations were performed for $T = 300$ K. The shapes of the doping profiles used in the calculations were adopted from the Secondary-Ion Mass Spectrometry (SIMS)-data for the fabricated diode. The raw experimental and the interpolated smoothed doping profiles are shown in Fig. 1a by dotted and solid lines, respectively. As can be seen from Fig. 1a, the whole diode contains three heavily doped regions. The left edge of the diode is strongly doped with As donor impurity with the peak concentration of ~1.5 × 10$^{21}$ cm$^{-3}$. The formed $n^{++}$-region extends by ~0.25 μm from the left diode edge. The first $p^+$-region is formed by B-doping with the peak concentration of ~ 1 × 10$^{17}$ cm$^{-3}$ at a distance of ~1.6 μm from the left diode edge. The second $p^{++}$-region with the peak concentration of ~1 × 10$^{19}$ cm$^{-3}$ is formed near the right edge of the diode. The raw data (dotted lines) were interpolated by smooth analytic functions. Particularly, the profiles at the edges were interpolated by the function $f(x) = r_0[\tanh(a(b-x))+1]/[\tanh(ab)+1]$ with $x$, $a$ and $b$ expressed in microns. The best fitting parameters for the donor profile, $N_d(x)$ are $r_0 = 1.65 \times 10^{21}$ cm$^{-3}$, $a = 60$ and $b = 0.07$. For the second acceptor profile, $N_a^{(2)}(x)$, the fitting parameters are $r_0 = 3.2 \times 10^{19}$ cm$^{-3}$, $a = 5.2$ and $b = 379.5$. The first acceptor profile, $N_a^{(1)}(x)$, was interpolated by a Gauss-type function, $f(x) = r_0 \exp\left(-0.5\left[\frac{x-b}{a}\right]^2\right)$, with $r_0 = 1.11\times10^{17}$ cm$^{-3}$, $a = 0.1$ and $b = 1.56$.

Using these interpolated doping profiles, we have calculated the distributions of the electrostatic potential

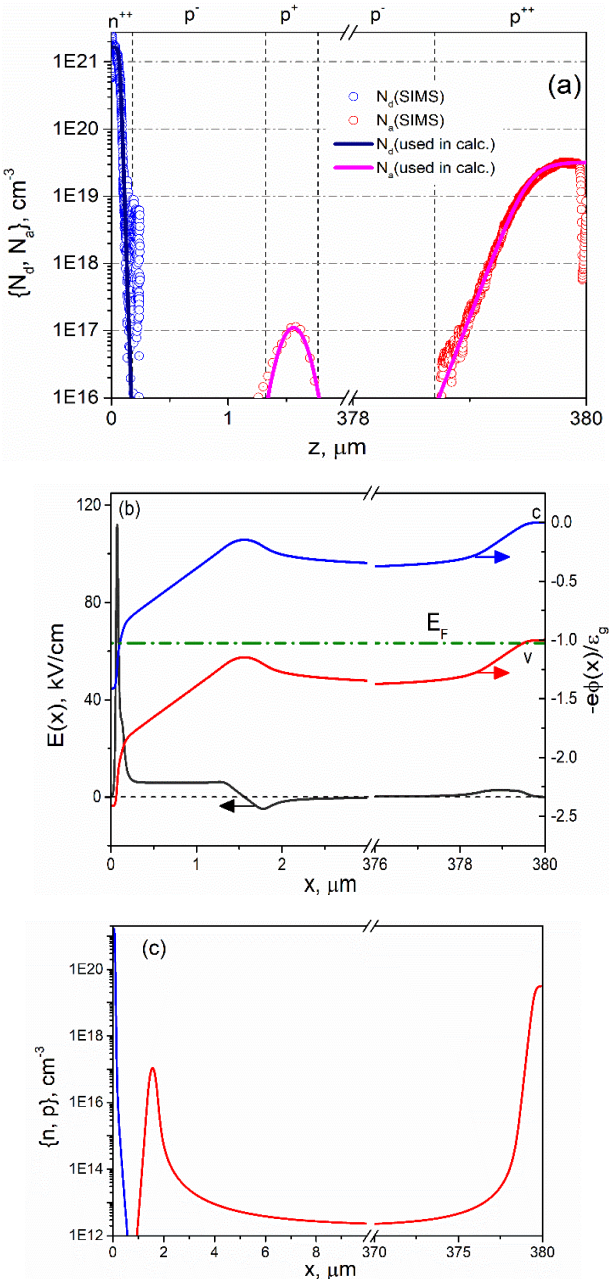


**Fig. 1.** (a) SIMS-measured (dots) and interpolated (lines) doping profiles of the fabricated Si diode. (b) Calculated band bending (right axis) and distribution of the electrostatic field (left axis) across the diode. The dash-dotted line depicts the Fermi-level position. (c) Calculated distributions of the electron (blue line) and hole (red line) concentrations. The results are shown for equilibrium state, $U_b = 0$.

(or band bending diagram), the built-in electrostatic field (see Fig. 1b) as well as the carrier concentration distributions (see Fig. 1c) under equilibrium. As can be seen from these figures, strong band bending and non-monotonic behavior of the electrostatic potential are observed in the $n^{++}$-$p^-$-$p^+$ junctions region that extends by ~2 μm from the left edge. The two slopes in the distribution of the electrostatic potential are clearly visible. The first rapid slope corresponds to the $n^{++}$-$p^-$ junction, where

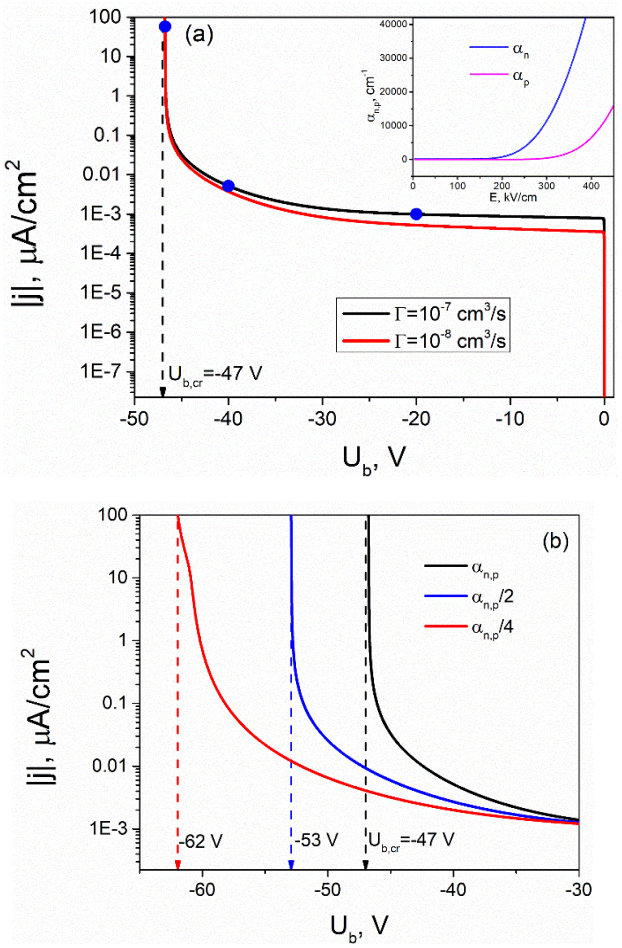


**Fig. 2.** *I–V* characteristics of the Si-based avalanche diode calculated at two values of the bulk recombination coefficient (a), and three dependences of the coefficients $\alpha_{n,p}$ (b). The inset in panel (a) shows the field dependences of the impact ionization coefficients given by Eqs. (11a) and (11b).

a strong built-in electrostatic field with the peak intensity of ~110 kV/cm is formed (see black curve in Fig. 1b). Note that such values can already lead to initiation of impact ionization. The second more extended and weaker slope corresponds to the depletion (or space-charge) region that is formed between the $n^{++}$- and $p^{+}$-regions (see Fig. 1c). Here, the electrostatic field has almost flat distribution with the characteristic value of ~5 kV/cm.

The results of the calculations of current-voltage (*I–V*) characteristics are presented in Fig. 2. The most attention was paid to the reverse branch of the *I–V* characteristics. The following interpolated field dependences of the impact ionization coefficients according to Refs. [2, 4] have been used in the calculations:

$$\alpha_n(E) = 3.8\times10^6 \exp\left(-\frac{1.75\times10^3}{E}\right), \qquad (11a)$$

$$\alpha_p(E) = 2.25\times10^7 \exp\left(-\frac{3.26\times10^3}{E}\right). \qquad (11b)$$

Here, the coefficients $\alpha_{n,p}(E)$ are expressed in $cm^{-1}$ and the field $E$ in kV/cm.

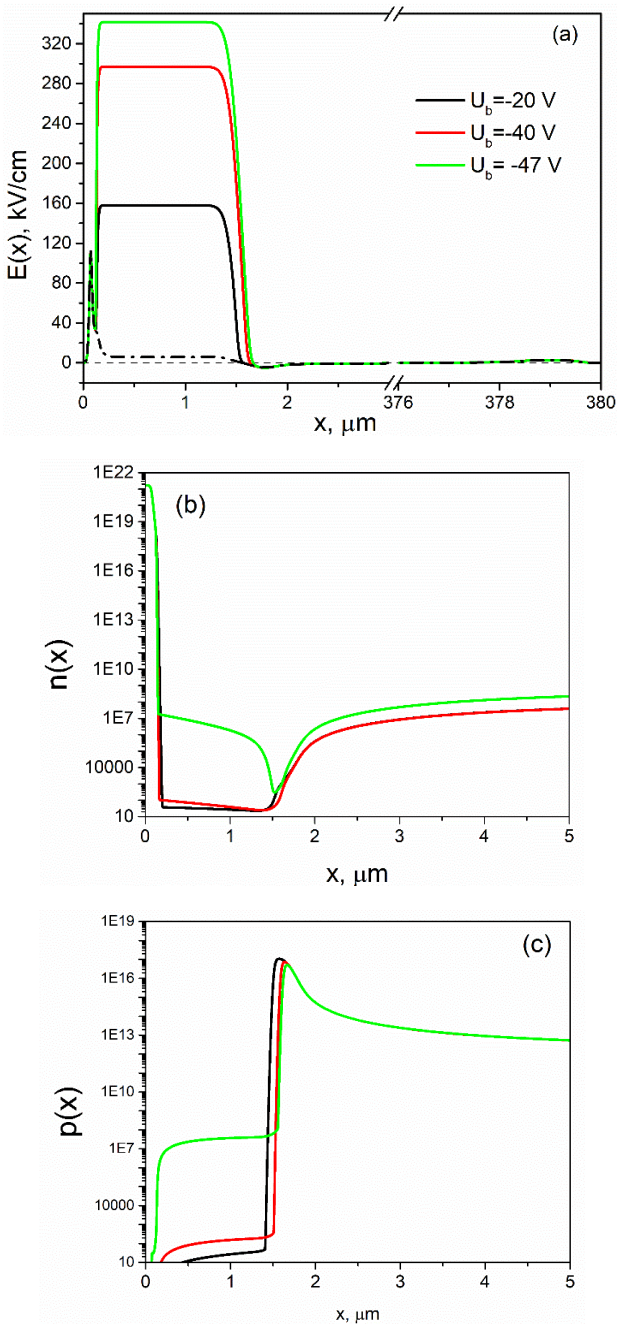


**Fig. 3.** Electric field (a), electron concentration (b), and hole concentration (c) distributions calculated at three values of the applied voltage: $U_b$ = –20, –40, and –47 V. The dash-dotted line in panel (a) corresponds to $U_b$ = 0 V. The corresponding current values are marked with blue dots in Fig. 2a.

As can be seen from Fig. 2a, the obtained theoretical *I–V* characteristics demonstrate a typical for *p-n* junctions saturated behavior in the wide range of the applied voltages, $U_b$ = –1…–40 V. Here, the current densities have the values of ~1…10 nA/cm$^2$. Initiation of the impact ionization effect starts from the applied voltages $U_b \lesssim$ –40 V. Further increase of $|U_b|$ leads to rapid exponential growth of the current density and avalanche-type regime of carrier transport in the diode.

For the selected geometry and chosen parameters of the diode, the calculations predict the critical threshold voltage for electrical breakdown $U_{b,\,cr}$ = –47 V. Note that this voltage is independent on the recombination parameter Γ (compare black and red curves in Fig. 2a). However, the critical voltage essentially depends on the parameters of impact ionization as illustrated in Fig. 2b. The absolute value of critical voltage increases with the decrease of the $\alpha_{n,p}$-coefficients.

Formation of an avalanche-type transport regime is clearly illustrated by distributions of the electric field in Fig. 3a as well as the carrier concentrations in Figs. 3b and 3c calculated at three values of the applied voltage: $U_b$ = –20, –40, and –47 V shown by blue dots in Fig. 2.

The obtained distributions indicate that an avalanche region is formed in the depletion region between the $n^{++}$- and $p^{+}$-parts of the diode in the range of $x$ = 0.5…1.6 μm. Here, a strong electric field reaching the value of 340 kV/cm (at $U_b$ = –47 V) and a rapid increase of the carrier concentrations (see green curves in Fig. 3) are obtained. Such value of the electric field corresponds to an exponential growth of the impact ionization coefficients shown in the inset in Fig. 2.

**4. Photoelectric characteristics**

In general, the proposed theoretical model and obtained numerical results are well-agreed with physics of avalanche diodes and well-correlated with early-obtained analytical results (see, for example, Ref. [2]). Moreover, the proposed model may be applied for an arbitrary geometry of doping profiles and may be easily adopted for the case of external illuminations with the aim of calculating photo-electrical characteristics. For this purpose, an additional generation term, $-G_\lambda$, has to be added into the right-hand side of Eq. (5e). This term is given by the following expression:

$$G_\lambda = \frac{I_\lambda \eta_\lambda}{\eta\omega} W_\lambda(x), \tag{12}$$

where $I_\lambda$ and $\omega = 2\pi c/\lambda$ are the flux density and frequency of the incident electromagnetic radiation with the wavelength λ, $\eta_\lambda$ is the quantum efficiency, and $\hbar$ and $c$ are the reduced Planck constant and light velocity in the vacuum, respectively. $W_\lambda(x)$ is the spatial distribution of the part of electromagnetic energy absorbed in the diode material per unit length. For spatially uniform semiconductor wafer of the finite thickness $L_b$, this quantity can be calculated as follows:

$$W_\lambda(x) = \frac{\omega}{c}\mathrm{Im}[\kappa_\lambda]\times \left| \frac{\cos\left(\frac{2\pi\sqrt{\kappa_\lambda^*}[L_b - x]}{\lambda}\right) - \frac{i}{\sqrt{\kappa_\lambda^*}}\sin\left(\frac{2\pi\sqrt{\kappa_\lambda^*}[L_b - x]}{\lambda}\right)}{\cos\left(\frac{2\pi\sqrt{\kappa_\lambda^*}L_b}{\lambda}\right) - i\frac{\kappa_\lambda^* + 1}{2\sqrt{\kappa_\lambda^*}}\sin\left(\frac{2\pi\sqrt{\kappa_\lambda^*}L_b}{\lambda}\right)} \right|^2 \tag{13}$$

Here, $\kappa_\lambda^* = \mathrm{Re}\left[\kappa_\lambda^*\right] + i\,\mathrm{Im}\left[\kappa_\lambda^*\right]$ is the complex *optical* permittivity, corresponding to indirect band-to-band transitions in silicon. Note that these formulas are written for the case of normal incidence of external radiation.

Using the photo-generation term (12) properly incurporated into the system (5), together with the distribution $W_\lambda(x)$ (13), we have calculated the photo *I–V* characteristics $j_{ph}(U_b)$ (shown in Fig. 4a) and responsivity $R_\lambda(U_b)$ (shown in Fig. 4b). The latter is defined as

$$R_\lambda(U_b) = \left| j_{ph}(U_b) - j(U_b) \right| \Big/ I_\lambda . \tag{14}$$

Here, $j(U_b)$ is the *dark* current density calculated without illumination (see Section 3). Calculations of the photoelectric characteristics were performed at $I_\lambda$ = 0.1 μW/cm$^2$ and three incidence radiation wavelengths, λ = 0.8 μm (blue curves), λ = 0.9 μm (red curves), and λ = 1 μm (black curves). The following values of $\kappa_\lambda^*$ were used for these wavelengths: $\kappa_{0.8}^* = 13.5 + i0.04$, $\kappa_{0.9}^* = 13.06 + i0.015$ and $\kappa_{1.0}^* = 12.75 + i0.0036$. The spectra of both parts of the optical permittivity in the near-IR spectral range (according to the novel database [10]) are presented in the inset (I) in Fig. 3a. We can see from this figure that silicon has a weak absorption capacity for electromagnetic waves of the considered spectral range. The imaginary part of $\kappa_\lambda^*$ is 2-3 orders smaller as compared to the real part of $\kappa_\lambda^*$, which is almost constant and equal to ~13. The distributions of $W_\lambda(x)$ shown in the inset (II) in Fig. 4a indicate the characteristic length $L_{ph}$ of penetration of electromagnetic waves into the silicon crystal. For all the assumed wavelengths, $L_{ph}$ is much larger than the thickness of the *p-n* junctions (space-charge region). We have estimated that $L_{ph}$ ~20…30 μm at λ = 0.8 μm, $L_{ph}$ ~ 100 μm at λ = 0.9 μm, and at λ = 1 μm, $L_{ph}$ becomes comparable with the total thickness of the diode $L_b$. At this, we observe an oscillating behavior of $W_\lambda(x)$ corresponding to the Fabri–Perot interference effect.

Our calculations predict rather good photoelectric sensitivity of the avalanche diode even to small portions of incident electromagnetic energy. For the flux density $I_\lambda$ = 0.1 μW/cm$^2$, the photocurrent calculated at λ = 1 μm (see the main panel in Fig. 4), is twice as large as the dark current. With the decrease of wavelength, the absorption capacity of silicon increases and, as a result, the values of the photocurrent also increase. At λ = 0.8 μm, $j_{ph}$ is approximately one order larger than the dark current. These observations are valid for a wide range of subthreshold voltages, $U_b$ = 0…–40 V. In this range, the responsivity of the diode (see Fig. 4b) does not exceed 0.1 A/W. However, the situation dramatically improves at approaching to the critical voltage of avalanche transport regime. The responsivity of the avalanche diode increases by three orders of magnitude and $R_\lambda$ reaches the values of 30 to 100 A/W in the narrow range of applied voltages, $U_b$ = –46.5…–47 V (see inset in Fig. 4b).

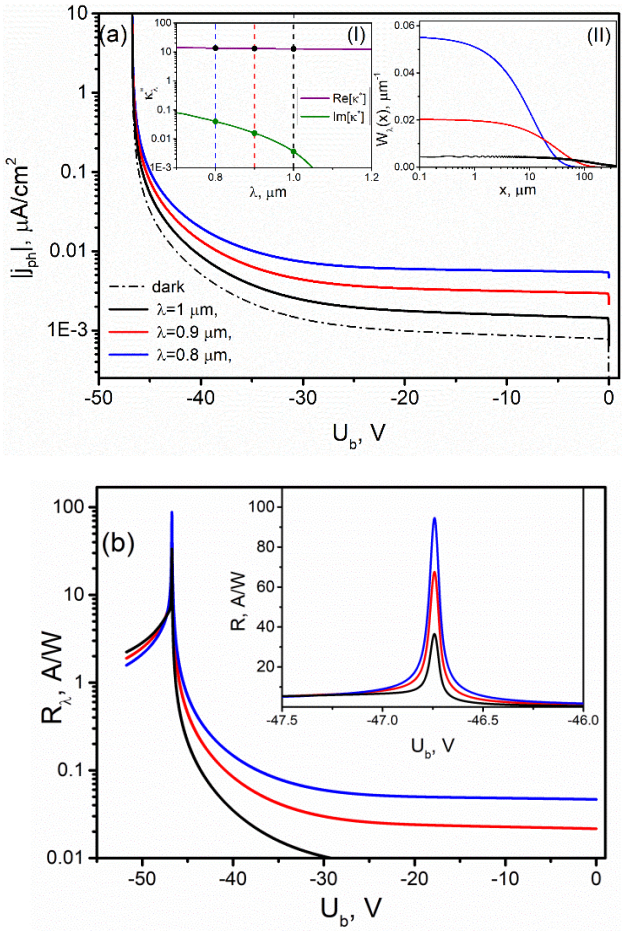


**Fig. 4.** (a) Photo-current density $j_{ph}$ *vs* applied voltage $U_b$ calculated at three values of the incident radiation wavelength. Dash-dotted line is the dark *I–V* characteristic. Inset (I): near-IR spectra of the optical permittivity taken from Ref. [9]. Inset (II): spatial distributions of $W_\lambda(x)$ in a 380 μm thick silicon wafer. (b) The corresponding voltage dependences of the responsivity $R_\lambda(U_b)$. Inset magnifies the region of the rapid increase of the responsivity.

Thus, our calculations emphasize the advantages of the avalanche diode over conventional *p-n* diodes with respect to detectivity of electromagnetic radiation in the near-IR spectral range [11]. An additional increase in the diode photoresponse can be achieved by using various types of optical metasurfaces [12, 13], which allow focusing IR radiation on the avalanche region.

## 5. Summary

In summary, we have developed a self-consistent theoretical approach for numerical modeling of the basic electric and photoelectric characteristics of Si-based avalanche diodes with specific $n^{++}$-$p^{-}$-$p^{+}$-$p^{-}$-$p^{++}$ doping profiles. In the framework of the proposed model, we found that the avalanche transport regime is realized at the reverse voltage of ~ 47 V applied across the diode length of 380 μm. This regime is described by formation of the avalanche region between the $n^{++}$- and $p^{+}$-parts of the diode, where a strong electric field of the order of ~ 300 kV/cm, sufficient for impact ionization, can be formed. At this, the *I–V* characteristics demonstrate rapid exponential growth at increasing the current density by 3-4 orders of magnitude. We have also investigated the diode photoresponse to electromagnetic radiation in the near-IR spectral range (λ = 0.8…1 μm). We have discovered that the diode performance with respect to photoresponse strongly depends on the radiation wavelength and the applied steady-state voltage. In the sub-threshold transport regime, $|U_b| < 30$ V, the diode responsivity does not exceed 0.1 A/W at λ = 0.8 μm and 0.01 A/W at λ = 1 μm. The responsivity of the diode rapidly grows with a further increase of $|U_b|$ and transition to the avalanche-type transport regime. We have found that in a narrow range of the applied voltages (near $U_{cr}$), the responsivity can reach high values of 100 A/W at λ = 0.8 μm and 30 A/W at λ = 1 μm. We suggest that the developed theoretical approach and performed analysis of electric and photoelectric characteristics of the Si-based avalanche photodiode will be useful for fabricating and testing working photo-detectors for the near-IR spectral range.

## Acknowledgments

This work was supported by the National Research Foundation of Ukraine (Grant No. 2022.01/0131, "Development of the latest manufacturing technology of a silicon avalanche photodiode for the near-infrared region of the spectrum").

## References

1. Capasso F. Physics of avalanche photodiodes. *Semiconductors and Semimetals*. 1985. **22**, Part D. P. 1–172. https://doi.org/10.1016/S0080-8784(08)62952-X.
2. Kaneda T. Silicon and germanium avalanche photodiodes. *Semiconductors and Semimetals*. 1985. **22**, Part D. P. 247–328. https://doi.org/10.1016/S0080-8784(08)62954-3.
3. Wegrzecka I., Wegrzecki M., Grynglas M. *et al.* Design and properties of silicon avalanche photodiodes. *Opto-Electron. Rev.* 2004. **12**. P. 95–104.
4. Lee C.A., Logan R.A., Batdorf R.L., Wiegmann W. Ionization rates of holes and electrons in silicon. *Phys. Rev.* 1964. **134**, No 3A. P. A761–A773. https://doi.org/10.1103/PhysRev.134.A761.
5. Tager A.S., Wald-Perlov V.M. *Avalanche-Transit Diodes and their Application in Microwave Technology*. M.: Sov. Radio, 1968.
6. Gribnikov Z.S. Quasi-drifting asymptotics of distribution function in semiconductors. *Fiz. Tekh. Poluprov*. 1981. **15**, No 7. P. 1372–1379.
7. Dmitriev A.P., Mikhailova V.P., Yassievich I.N. Impact ionization in $A^{III}B^{V}$ semiconductors in high electric fields. *phys. status solidi* (*b*). 1987. **140**, No 1. P. 9–37. https://doi.org/10.1002/pssb.2221400102.
8. Korotyeyev V.V., Kochelap V.O., Sapon S.V. *et al.* Be-ion implanted *p-n* InSb diode for infrared applications. Modeling, fabrication and characterization. *SPQEO*. 2018. **21**. P. 294–306. https://doi.org/10.15407/spqeo21.03.294.

9. Levinstein M., Rumyantsev S., Shur M. *Handbook Series on Semiconductor Parameters*. **1**. World Scientific Publ., 1996.
10. Polyanskiy M.N. Refractiveindex.info database of optical constants. *Sci Data*. 2024. **11**. P. 94. https://doi.org/10.1038/s41597-023-02898-2.
11. Tanabe M., Amemiya K., Numata T., Fukuda D. Spectral supralinearity prediction of silicon photodiodes in the near-infrared range. *Appl. Opt.* 2015. **54**. P. 10705–10710. http://doi.org/10.1364/AO.54.010705.
12. Zang K., Jiang X., Huo Y. *et al.* Silicon single-photon avalanche diodes with nano-structured light trapping. *Nat. Commun.* 2017. **8**. P. 628. https://doi.org/10.1038/s41467-017-00733-y.
13. Gao Y., Cansizoglu H., Polat K. *et al*. Photon-trapping microstructures enable high-speed high-efficiency silicon photodiodes. *Nature Photon*. 2017. **11**. P. 301–308. https://doi.org/10.1038/nphoton.2017.37.

**Authors and CV**

**Sergey V. Sapon**, Researcher and Head of the Technical Section at the V. Lashkaryov Institute of Semiconductor Physics. His main research activities are microelectronic technologies for micro- and optoelectronics. Authored over 6 technical papers and patents of Ukraine.
E-mail: sergsapon58@gmail.com,
https://orcid.org/0000-0001-6134-6548

**Boris Romanyuk**, DSc in Physics and Mathematics, Professor, Head of the Department of Ion-Beam Engineering and Structural Analysis at the V. Lashkaryov Institute of Semiconductor Physics. Author of more than 270 scientific publications. His research interests include physics of semiconductors and dielectrics, ion-beam engineering and wide-range studies of semiconductor structures.
E-mail: romb@isp.kiev.ua,
https://orcid.org/0000-0002-1688-7588

**Oleksandr Dubikovskyi**, PhD in Physics and Mathematics, Researcher at the Department of Ion-Beam Engineering and Structural Analysis at the V. Lashkaryov Institute of Semiconductor Physics. He is the author of more than 16 publications. The main directions of his scientific activity are ion-beam modification and mass-spectrometry of semiconductor structures. E-mail: dubikovsky_o@ukr.net,
https://orcid.org/0000-0002-1504-8440

**Viktor Melnik**, DSc in Physics and Mathematics, Professor, Acting Director of the V. Lashkaryov Institute of Semiconductor Physics. Author of more than 250 scientific publications. His main research activity is in the fields of ion-beam engineering and diagnostics.
E-mail: vp_mel@ukr.net,
https://orcid.org/0000-0002-8670-7415

**Oleksandr A. Kulbachynskyi**, PhD Student at the Department of Ion-Beam Engineering and Structural Analysis of the V. Lashkaryov Institute of Semiconductor Physics. His main research activities are physics of thin films, chromogenic materials, SIMS analysis and ion implantation.
E-mail: s.kulbachynskyi@gmail.com,
https://orcid.org/0000-0001-6657-5569

**Oleksandr Oberemok**, PhD in Physics and Mathematics, Senior Researcher at the Center for the Collective Use of Scientific Instruments of the V. Lashkaryov Institute of Semiconductor Physics. He is the author of more than 50 publications. His main research activities are physics of surfaces, interfaces, nanoscale multilayer structures and thin films, and ion-beam engineering and diagnostics using SIMS, SNMS and GDMS. E-mail: ober@isp.kiev.ua,
https://orcid.org/0000-0003-2295-6209

**Zoia Maksimenko**, PhD in Physics and Mathematics, Researcher at the Department of Ion-beam Engineering and Structural Analysis of the V. Lashkaryov Institute of Semiconductor Physics. The main direction of her scientific activity is studying semiconductor nanostructures by high-resolution X-ray diffractometry in the field of anomalous X-ray dispersion. E-mail: ZMaksimenko@gmail.com,
https://orcid.org/0000-0002-3434-3728

**Oleksandr Kosulya**, PhD in Physics and Mathematics, Researcher at the Department of Ion-Beam Engineering and Structural Analysis, the V. Lashkaryov Institute of Semiconductor Physics. His research interests include secondary ion mass spectrometry, ion implantation, analysis of thin-film and multilayer structures, and analysis of chemical composition. E-mail: Alexandr250990@gmail. com,
https://orcid.org/0000-0001-7642-8052

**Vadym V. Korotyeyev**, DSc, Senior Researcher at the Department of Theoretical Physics, V. Lashkaryov Institute of Semiconductor Physics. His scientific interests include high-field and high-frequency electron transport in low-dimensional systems and nanoscale devices, Monte Carlo simulations, and generation and detection of THz radiation. Authored more than 70 scientific papers.
E-mail: koroteev@ukr.net,
https://orcid.org/0000-0002-0463-7872

**Valeriy N. Sokolov**, PhD in Physics and Mathematics, Senior Researcher at the Department of Theoretical Physics, V. Lashkaryov Institute of Semiconductor Physics. His scientific interests focus on quantum transport effects, noise phenomena in low-dimensional structures, and nanoscale devices and THz plasmonics.
E-mail: svaleriy721@gmail.com,
https://orcid.org/0000-0003-3211-6799

**Andrii V. Bychok**, Leading Design Engineer at the State Research Institute "Orion". The area of his scientific interests is development, design and manufacture of solid-state component base of microwave electronics for the short-wave part of the millimeter-wave spectral range for modern and advanced radio engineering devices.
E-mail: andrey.bychok@gmail.com

**Authors' contributions**

**Sapon S.V.:** conceptualization, investigation, supervision, writing – original draft.
**Romaniuk B.M.:** project administration, writing – review & edition.
**Melnik V.P.:** methodology, investigation, writing – original draft.
**Dubikovskyi O.V.:** investigation, visualization.
**Kulbachynskyi O.A.:** methodology, investigation.
**Oberemok O.S.:** resources, investigation.
**Maksimenko Z.V.:** visualization, writing – original draft.
**Kosulya O.V.:** methodology, investigation.
**Korotyeyev V.V.:** calculations, validation investigation, writing – original draft.
**Sokolov V.N.:** data analysis, methodology, investigation.
**Bychok A.V.:** investigation, formal analysis.

**Лавинний діод на основі Si $n^{++}$-$p^{-}$-$p^{+}$-$p^{-}$-$p^{++}$: самоузгоджене моделювання для інфрачервоних оптоелектронних застосувань**

**С.В. Сапон, Б.М. Романюк, В.П. Мельник, О.В. Дубіковський, О.А. Кульбачинський, О.С. Оберемок, З.В. Максименко, О.В. Косуля, В.В. Коротєєв, В.Н. Соколов, А.В. Бичок**

**Анотація.** Запропоновано теоретичний підхід для моделювання електричних та фотоелектричних характеристик кремнієвого лавинно-пролітного діода зі складним $n^{++}$-$p^{-}$-$p^{+}$-$p^{-}$-$p^{++}$ профілем легування. Було розраховано електростатичні (вигин зон, розподіли вбудованих електричних полів та носіїв заряду) та вольт-амперні характеристики діода включно з фотострумами та функцією відгуку на електромагнітне випромінювання ближнього інфрачервоного спектрального діапазону при робочих кімнатних температурах. Розрахунки проведено при конкретних профілях легування виготовленого прототипу кремнієвого діода. У запропонованій моделі було отримано, що лавинний режим транспорту носіїв реалізується при зворотних прикладених напругах ~ –47 V на довжину діодної області 380 мкм. Цей режим транспорту характеризується швидким експоненціальним зростанням густини струму від 0.01 до 100 мкА/см$^2$ у діапазоні прикладених напруг –40…–47 В. При цьому фотовідгук діода прогнозується в інтервалі 100…30 А/В для електромагнітного випромінювання з довжинами хвиль 0.8..1 мкм. Усі результати було отримано з використанням літературних даних щодо польових залежностей коефіцієнтів ударної іонізації, спектральних залежностей оптичної проникності (показника заломлення та екстинкції), тощо.

**Ключові слова:** фотодіод на основі Si, вольт-амперні характеристики, фотовідгук, імплантація.